Biosensors and Bioelectronics 137 (2019) 123–132

Contents lists available at ScienceDirect

Biosensors and Bioelectronics

journal homepage: www.elsevier.com/locate/bios

Impedimetric aptasensor for the label-free and selective detection of Interleukin-6 for colorectal cancer screening

Mihaela Tertis[a], Petrica Ionut Leva[a], Diana Bogdan[b], Maria Suciu[b,c], Florin Graur[d,e,**], Cecilia Cristea[a,*]

[a] Department of Analytical Chemistry, Faculty of Pharmacy, "Iuliu Hatieganu" University of Medicine and Pharmacy, 4 Louis Pasteur St, 400349, Cluj-Napoca, Romania
[b] National Institute for Research and Development of Isotopic and Molecular Technologies, 67-103 Donat St., 400293, Cluj-Napoca, Romania
[c] Faculty of Biology and Geology, Babes-Bolyai University, 5-7 Clinicilor St, 400006, Cluj- Napoca, Romania
[d] Department of Surgery, Faculty of General Medicine, "Iuliu Hatieganu" University of Medicine and Pharmacy Cluj-Napoca, 4 Louis Pasteur St., 400349, Cluj-Napoca, Romania
[e] Regional Institute of Gastroenterology and Hepatology "Octavian Fodor" Cluj-Napoca, 19-21, Croitorilor St, Cluj-Napoca, Romania

ARTICLE INFO

Keywords:
Biosensors
Aptamers
Nanoparticles
Interleukin-6
Label-free detection

ABSTRACT:

Despite the fact that cancer research has experienced important advances and remarkable improvement in the curing processes during the last decades, this disease still occupies a leading position among the causes of death worldwide. It has been demonstrated that there is an interconnection between the overexpression of interleukin-6 cytokine and the tumor growth, metastasis, and therapeutic resistance in several types of malignancies.

Herein, a highly sensitive and selective aptasensor for quantitative detection of interleukin-6 was developed by using a glassy carbon electrode modified with *p*-aminobenzoic acid, *p*-aminothiophenol and gold nanoparticles. A thio-terminated aptamer specific for interleukin-6 was immobilized on the surface of the modified electrode *via* the formation of gold-sulfur bonds. This DNA oligonucleotide was then used as a detection probe to capture the target protein at the biosensor surface allowing label-free detection by electrochemical impedance spectroscopy. The developed aptasensor showed a good linear response from 5 $pgmL^{-1}$ to 100 $ngmL^{-1}$ with a detection limit of 1.6 $pgmL^{-1}$, within the range of physiological concentration of the protein. The biosensor exhibited high selectivity and has been successfully used to detect interleukin-6 in blood samples collected from patients suffering of colorectal cancer, with excellent recoveries after the addition of known amount of the target protein.

1. Introduction

Being highly soluble in biological fluids, cytokines are a category of circulating proteins that can be detected in serum, saliva and other biological fluids and their levels are correlated with clinical features and survival rate (Fayad et al., 2001; Xue et al., 2015). Interleukin-6 (IL-6) is a multifunctional cytokine that influences the activity of cancer cells. It is a glycoprotein which consists of 184 amino acids and has molecular weight of 26 kDa (Zarogoulidis et al., 2013). Furthermore, IL-6 is one of the major cytokines which is found at high concentrations and known to be dysregulated in cancer. Its overexpression has been reported in almost all types of tumors being involved in tumor genesis, growth, and malignant differentiation of cancer cells, tumor microenvironment, immunomodulation and metabolism (Le Saout et al., 2012). The strong association between inflammation and cancer is reflected by the high IL-6 levels in the tumor microenvironment (Kumari et al., 2016; Chang et al., 2013; Pine et al., 2011; Lagiou et al., 2011).

Sensitive fast and accurate detection of biomarker proteins, including IL-6, is very challenging, mainly due to its very low concentration released in the extracellular environment. Despite this, IL-6 detection is highly desirable since it is linked with the possibility of diagnosing the progression of many diseases and to assess the response to particular treatments (Liu et al., 2016). The enzyme-linked immunosorbent assay (ELISA) and chemiluminescence immunoassay) (CLIA) are the conventional method used for proteins quantification, allowing limits of detection of $pgmL^{-1}$ (Hanash et al., 2008; Malhotra et al., 2010). However, both ELISA and CLIA have limitations in terms of analysis time, multiplexing, sample volume, and even in sensitivity

* Coressponding author.
** Corresponding author. Department of Surgery, Faculty of General Medicine, "Iuliu Hatieganu" University of Medicine and Pharmacy Cluj-Napoca, 4 Louis Pasteur St., 400349, Cluj-Napoca, Romania.
E-mail addresses: florin.graur@umfcluj.ro (F. Graur), ccristea@umfcluj.ro (C. Cristea).

https://doi.org/10.1016/j.bios.2019.05.012
Received 10 February 2019; Received in revised form 8 April 2019; Accepted 4 May 2019
Available online 07 May 2019
0956-5663/

for some particular analytes. Alternative approaches for IL-6 sensitive detection include other strategies such as multiplexed immunoassay based on nanoplasmonic biosensor microarrays (Chen et al., 2015), fluorescence (Hendricks et al., 2000), surface plasmon resonance (Malhotra et al., 2010) and electrochemical (bio)sensors (Selva Kumar et al., 2016; Tertiş et al., 2017b).

Several electrochemical biosensors have been elaborated and applied for medical and environmental assessments due to their favorable characteristics, such as fast, cheap and sensitive analysis, as well as the compatibility for on-site decentralized analysis and miniaturization (Mazerie et al., 2018; Roushani and Shahdost-fard, 2015). In the case of solid, flat electrodes, the analytical performance might be drastically reduced by the occurrence of a phenomenon called fouling. The electrode surface reduces the rate of electron transfer and implicit the analytical signal. A useful alternative is represented by the enhancement of the active surface area of the electrode after functionalization with nanomaterials (nanotubes, graphene, gold nanoparticles (AuNPs), etc.) (Tertiş et al., 2017b; Roushani and Shahdost-fard, 2015; Tertiş et al., 2013; Cernat et al., 2015; Fritea et al., 2015a; Fritea et al., 2015b; Tertis et al., 2017c; Tertis et al., 2017a; Cernat et al., 2018), strategy that allows to design sensors with increased sensitivity. In addition to this, a trend consisting in the employment of nanocomposites with tridimensional structures has recently empowered the development of highly sensitive bio-medical diagnostic devices. For example, several nanocomposites with tridimensional structures have been successfully synthesized such as hydroxyapatite ($Ca_{10}(PO_4)_6(OH)_2$) nanorods, nanobundles and nanoparticles (Mohandes et al., 2014), magnetic rod-like platelet of $NiFe_2O_4$ (Amiri et al., 2018b), nanoparticles of $CoFe_2O_4$ (Amiri et al., 2018a), spinel-type nanocomposite of $CoFe_2O_4/SiO_2$ (Mahnaz Amiri et al., 2017), rare earth zirconates ($Ln_2Zr_2O_7$) (Zinatloo-Ajabshir et al., 2018) or metallic nanostructures (Qazi et al., 2016) for biomedical applications.

Aptamers (Apt) are oligonucleotides obtained by the process of systematic evolution of ligands by exponential enrichment (SELEX) that bind their targets with high affinity and specificity (Gupta et al., 2014). Considering their features, Apt have been used for a wide range of both *in vitro* and *in vivo* applications, including affinity chromatography, microscopy, and biomarker identification (Gupta et al., 2011; Gold et al., 2010).

A good strategy for increasing the amount of aptamer molecules immobilized on the electrode surface is represented by the use of metal nanoparticles. If it is chosen to employ these materials, it is crucial to ensure that they are fixed on the surface of the substrate material to avoid their detachment during the developing of the aptasensor. Gold nanoparticles (AuNPs) were of particular interest in this field and have been widely used as immobilization matrix in biosensors fabrication for enhancing their performance (Qazi et al., 2016).

Herein, a novel aptasensor for IL-6 detection based on glassy carbon electrode (GCE) was reported. This transducing support was used for the covalent immobilization of AuNPs *via* self-assembling process of *p*-aminothiophenol (pATP) which was previously anchored by the amide bond on the *p*-aminobenzoic acid (pABA) film electrochemically grafted on the electrode.

Various other methods have been used over time to functionalize and improve the analytical properties of the electrode surfaces with organic and inorganic compounds or to increase their selectivity and sensitivity by further immobilization of biocomponents and biomimetic elements. For example, mussel-inspired surface chemistry has emerged as one of the most interesting routes for fabrication of functional materials. In this respect, the use of polydopamine has been reported since this coating facilitates a variety of reactions with organic and inorganic species. Although this type of functionalization has numerous advantages (Zhang et al., 2017) (Huang et al., 2017), for the present study has been chose the controlled production of carboxyl groups on the electrode surface using pABA because it facilitates the controlled immobilization of pATF molecules through amide bond formation. Thus, the remaining thio groups are available on the surface of the composite film for the subsequent immobilization of AuNPs from suspension. This immobilization strategy for AuNPs has been previously reported (Zhang et al., 2005; Pilehvar et al., 2017), but the protocol was adapted for ssDNA oligonucleotide with high affinity for IL-6.

Different strategies have been used so far for the Apt immobilization. For example, hemin, graphene oxide and multi-walled carbon nanotubes modified glassy carbon electrode was obtained and used for Apt immobilization through amidic covalent bonds (Mazloum-Ardakani et al., 2019). Another widely used strategy for Apt immobilization at the transducer surface is represented by its self-assembling through the formation of strong bounding between thiol and gold (Yang et al., 2018); (Chen et al., 2019; Tertiş et al., 2017b). The last presented immobilization strategy of the biomimetic element was applied in the current study. This optimized experimental strategy offered a repeatable and stable immobilization for the Apt and provided perfect conditions for the protein capture. One of the novel features of this study is represented by using this type of immobilization for big targets like proteins, which has not been reported before. The collective benefits of AuNPs covalent binding and a fast and sensitive label-free IL-6 protein electrochemical detection is demonstrated for the first time here, as a potential for colorectal cancer screening.

2. Experimental section

2.1. Reagents, instruments and procedures for solution preparation and testing

All the reagents and solvents used for this study were of analytical grade, and were used as received. All the aqueous solutions were prepared using ultrapure water (18 $M\Omega cm^{-1}$). More details about the reagents provenience and characteristics, instruments and experimental procedures are presented in *Supplementary data* (S2.1).

2.2. Aptasensor elaboration protocol

Firstly, GCE was functionalized with *p*-ABA by cycling the potential from −1 to +1 V/AgAgCl(KCl, 3M) for 5 cycles at a scan rate of 50 mV s^{-1}. The activation step with NHS/EDC mixture was then performed by contacting the electrodes with this solution for 30 min, to facilitate the amidic bond formation between the carboxyl group at the electrode and the amino group of pATP. The electrode was then incubated with 1.5 $mmolL^{-1}$ pATP solution for 30 min, this step being followed by the 30 min immobilization of AuNPs from a homogenous solution prepared in citrate buffer. The 3′-thiolated IL-6 specific Apt molecules (oligonucleotide sequence: 5′-GTC TCT GTG TGC GCC AGA GAC ACT GGG GCA GAT ATG GGC CAG CAC AGA ATG AGG CCC-3′) were immobilized at the electrode through sulfur-gold bonding (60 min incubation with 1.5 $\mu molL^{-1}$ Apt solution at room temperature). The surface of the AuNPs that remains unoccupied with Apt was further blocked with mercaptohexanol (MCH) to avoid non-specific adsorption (30 min incubation with 1 $mmolL^{-1}$ MCH solution at 4 °C). In the next step, the IL-6 protein was immobilized from synthetic and real samples after 60 min incubation at room temperature.

2.3. Interference study and real samples analysis

Blood samples (~5 mL) were clinically collected from three patients suffering from colorectal cancer (diagnosis was confirmed histopathologically, all the patients being subsequently operated for this pathology). The blood sampling was performed prior to administration of any treatment and before the anaesthesia, in order to avoid the influence or alter the levels of IL-6. Patients' consents were obtained prior the sampling procedure and all institutional recommendations on handling real samples taken from human subjects were followed (under the agreement of the Ethics Committee No.2316/19.03.2018) More

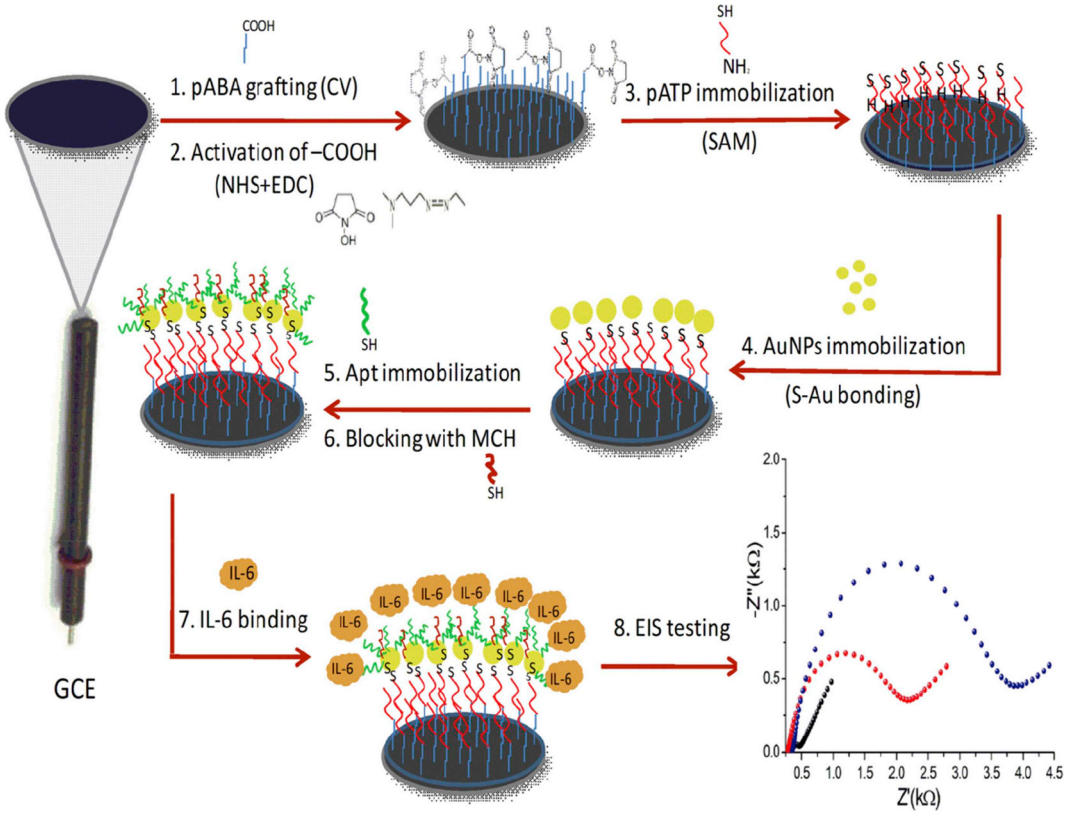

Fig. 1. Schematic representation of the aptasensor elaboration protocol and testing.

details in *Supplementary data* under the point S2.2.

3. Results and discussion

3.1. Design of the IL-6 aptasensor

The representation of the stepwise protocol applied for the modification of the GCE in order to succeed in IL-6 label-free aptasensing is represented in Fig. 1. Briefly, the electrochemical grafting of pABA was performed to generate the carboxyl functionalities. This step is important since these functionalities are further used for covalent immobilization of pATP through amidic bond. The presence of the pATP generates free thiol groups employed for the attachment of AuNPs (Pilehvar et al., 2017; Gobbo et al., 2012). The next step consists in the immobilization of a 3′-thiolated IL-6 specific Apt on the electrode *via* sulfur-gold bonding. The surface of the AuNPs that remains unoccupied with Apt was further blocked with MCH in order to avoid non-specific adsorption. Caused by target protein binding, a conformational change of Apt chain takes place. This process increases the signal registered by the analytical electrochemical impedance spectroscopy (EIS), in comparison with the results obtained in the absence of the target. This increase was quantified upon testing the optimized aptasensor with IL-6 solutions of different concentrations prepared in buffer or in human serum.

3.2. Optimization of the experimental protocol for the elaboration of the IL-6 aptasensor

The analytical performance of the electrochemical aptasensor was determined on the basis of a very optimized and detailed protocol. Several parameters were optimized, such as (1) the pABA grafting time and its concentration, (2) the concentration of the solution used for activation of carboxylic groups and (3) the time used for this process, (4) the concentration of pATP and (5) the time required for the self-assembling, (6) the concentration of AuNPs suspension and (7) the contact time between pATP and Apt, (8) the concentration of the Apt solution and (9) its incubation time, (10) the concentration of MCH solution and (11) the time required for the coverage of the free active sites available after Apt immobilization (to avoid the nonspecific adsorption), (12) the time and (13) temperature which lead to faster and optimum immobilization of the protein. CV (cyclic voltammetry) and/or EIS were mainly used for this optimization, excepting the case of immobilization of AuNPs on the pATP and of Apt on the gold surface. For these steps, UV–Vis spectroscopy was applied. The values for the each of the mentioned parameters were compared to the signal recorded for the previous step used for biosensor development. CV and EIS data obtained during the optimization protocol are summarized in Table 1, and the optimization for pATP and Apt immobilization are detailed in the following section.

3.2.1. Optimization of the pATP immobilization

The UV–Visible spectroscopy was used to confirm the formation of Au–S bonds between the pATP and the AuNPs from suspension. This step was important since the nanoparticles immobilized at the electrode were further helpful for the Apt immobilization. The spectroscopy graph was registered in the range 400–800 nm for solutions containing 100 μmolL^{-1} pATP and a 1:1 (V:V) ratio between the pATP solution and AuNPs suspension (1:1 dilution in 2 mmol L^{-1} citrate buffer pH 6.5) for different contact times. The values of the recorded spectra are presented in Figure S1(A). One can observe an absorption band with the maximum intensity at 542 nm, characteristic to AuNPs, confirming the possibility to gain information about the dimension and shape of Au nanostructures (Zhang et al., 2012). A decrease in the specific absorption intensity was registered upon increasing the contact time from 0 min to 12 h, confirming the formation of gold-sulfur bonds. The most important variation in AuNPs-specific absorbance was observed after 30 min, when it was observed an increase of about 19%, from 0.230 to 0.188 absorbance units. However, after 12 h incubation time, it was

Table 1
EIS and CV parameters obtained during aptasensor optimization.

Elaboration step	Optimized parameter		R_{ct}/kΩ	I_{ox}/μA
Immobilization of pABA	pABA solution concentration (1 mmol L^{-1}) Number of CV cycles (1 mmol L^{-1})	0.5	1.9 ± 0.03	165
		1	3.8 ± 0.08	108
		1.5	3.4 ± 0.11	106
		5	3.8 ± 0.08	108
		10	4.3 ± 0.13	92
Activation of COOH groups (NHS/EDC)	Time	15 min	0.91 ± 0.04	161
		30 min	1.78 ± 0.07	151
		45 min	2.18 ± 0.04	149
Immobilization of pATP (incubation)	pATP concentration (mmol L^{-1}) (30 min)	10	6.9 ± 0.13	–
		50	10.3 ± 0.21	
		100	9.13 ± 0.24	
Apt immobilization	Apt concentration (μmol L^{-1}) (30 min)	0.5	13.9 ± 0.26	–
		1	16.6 ± 0.31	
		1.5	23.9 ± 0.54	
	Temperature (1.5 μmol L^{-1}) (30 min)	4 °C	18.8 ± 0.38	–
		25 °C	23.9 ± 0.54	
		37 °C	24.3 ± 0.47	
Blocking with MCH (1 mmol L^{-1}) Incubation time	Time (4 °C)	15 min	24.1 ± 0.31	–
		30 min	25.3 ± 0.29	
		60 min	26.6 ± 0.63	
IL6 protein immobilization (2 ng mL^{-1})Incubation time	Time (25 °C)	30 min	31.5 ± 0.82	–
		60 min	48.8 ± 1.14	
	Temperature (60 min)	4 °C	33.9 ± 0.91	–
		25 °C	48.8 ± 1.14	
		37 °C	46.3 ± 2.06	

recorded a total decrease of about 32%. Thus, 30 min has been chosen as optimal contact time between AuNPs and pATP.

3.2.2. Optimization of the aptamer immobilization

The contact time needed for Apt molecules immobilization at the electrode was also studied with UV–Visible spectroscopy. For this purpose, the spectra were registered in both UV (to follow the characteristic band of Apt at 260 nm) and visible domain (for the characteristic band of AuNPs, having the absorption maximum at 542 nm). In Figure S1(B) is represented the different contact times registered (from 0 min to 12 h) for solutions containing 10 μmolL^{-1} Apt (green), a 1:10 AuNPs diluted suspension (orange) and 1:1 (V/V) mixture of an Apt solution and of an AuNPs suspension prepared to obtain the same concentration for the two species as in individual controls. The inset graph presented in Figure S1(B) is a zoom for the part of the spectra registered in visible domain. It can be observed that the intensity of the absorption band for both Apt and AuNPs decreases with the contact time, being an evidence for the immobilization of the biorecognition element at the gold surface. It was observed that after more than 60 min of contact, no significant differences were registered in the specific absorbance of AuNPs at 542 nm (a decrease of 58% being registered after 12 h, while after 60 min the decrease was about 56%). Thus 60 min was settled as optimal time for Apt immobilization.

3.3. Characterization of the IL-6 aptasensor

3.3.1. AFM, SEM, EDS and XPS characterization

AFM, SEM, EDS and XPS characterization of the GCE during all the modification steps have been performed to reveal the electrode surface morphology and its elemental composition. In the case of the unmodified GCE, the SEM images show a smooth conductive surface with few nanometer deep scratches (data not shown). The surface of pABA modified GCE has a uniform thin layer of pABA with the surplus gathered in fractal thicker layers of arborescent-like deposits (Fig. 2A(a) and Figure S2(A)). The surface of pABA and pATP has a different morphology altogether: it forms a continuous thin film (when inspected at nanometer size) but the surplus gathers in different-sized round emulsion-like material, uniformly dispersed on the glassy carbon (aspect visible at micron size analysis) (Fig. 2A(b) and Figure S2(B)). After the immobilization of AuNPs on the modified electrode, the SEM images shows round-shaped bright dots, that can be clearly assigned to AuNPs presence. In this case, the micro-scale surface shows a uniformly distributed material resembling the emulsion-like film from the former functionalization steps. At the nano-scale, the 50 nm AuNPs become visible, showing the appearance of shimmering spots surrounded by a halo, relatively uniformly distributed as single nanoparticles, although with a tendency to concentrate in the thicker deposited material. The AuNPs seem to be covered with a thin layer of pABA-pATP, as can be seen in Fig. 2A(c) and Figure S2(C).

This clearly proves that the modification of the electrode surface was obtained through the covalent binding, rather than nonspecific adsorption. The phenomenon can be attributed to the presence of different functionalities provided by the surface modifiers (pABA and pATP) that may hinder the AuNPs agglomeration and facilitate the improvement of the biosensor's analytical performance, as it was already observed (Zhang et al., 2005; Pilehvar et al., 2017; Shin and Kang, 2003; Erdem, 2007).

The EDS analysis could only reveal the presence of carbon and oxygen in the first three steps of the aptasensor elaboration (At%: GCE: C:O = 94.65:5.35; pABA/GCE: C:O = 94.4:5.6; pATP/pABA/GCE: C:O 91.25:8.75). After the immobilization of AuNPs, the analysis indicated the Au presence in an atomic percentage of C:O:Au = 92.2 : 7.8: 0.1.

AFM analysis highlights morphological changes of the electrode surface after each step of surface modification (Fig. 2B). AFM images of bare GCE surface show few nanometers deep straight scratches originating from polishing process (visible on large scan areas, 20 × 20 μm^2) (Figure S3(Athese fine lines, GCE surface is very smooth (root mean square roughness R_q 0.3 nm over 2 × 2 μm^2 area) (Fig. 2B(a)). The effect of modification with pATP/pABA appears as changes in morphology and topography of the electrode surface, that is now uniformly covered by the polymeric thin layer (R_q 1.3 nm over 2 × 2 μm^2 area), highlighted by some rounded (globular) features of different diameters (Fig. 2B(b) and Figure S3(B)). The particle-like features are uniformly distributed over the surface; on 2 × 2 μm^2 area. N = 110 particles were counted having diameters larger than 8 nm, which cover about 2.5% of the surface, more than 50% of them being in the range 10–12 nm. The AuNPs deposition on the final electrode (Fig. 2B(c) and Figure S3(C)) shows a relatively uniform distribution, with a tendency to form small aggregates of few nanoparticles characterized by 50 nm diameter, as clearly seen in the AFM images.

XPS tests performed for this study confirmed the success of the modification since the compositions of the film at the electrode was investigated with this technique. All the results of the XPS analysis were summarized in Tables S1-S4. Thus, it can be noticed that GCE naturally contains, besides sp^2 carbon, some amounts of nitrogen, oxygen and sulfur. Their origin is probably due to impurities existing before the formation of the glassy phase. After the formation of this phase they were fixed in the matrix mostly just below the surface. Also a smaller quantity of sp^3 carbon is present. Additionally, at binding energies of 285.63 and 287.68 eV there are carbon atoms belonging to, O-C-O and COOH groups respectively and carbon bind to nitrogen (C–N) at binding energy around 285 eV (Table S1). On the other hand, by analyzing the intensity of the XPS lines, one can see that the sp^2 intensity is practically the same for unmodified GCE and after the modification with p-ABA and p-ATP (Tables S1-S3). Thus, the absolute intensities of the other peaks can be directly compared with these ones. The presence of p-ABA has been proven through the increase of the C–N line intensity with about 40% with respect to unmodified GCE. Interestingly, a decrease in the intensity of the O-C-O peak (deprotonated COOH) indicates that the addition of polymer results in a *re*-protonation process. The presence of p-ATP is indicated by the four times increased line intensities of S 2*p* 3/2 and 1/2 thiol peaks positioned at 163.7 and 164.48 eV respectively (Table S3). This increase is relative to the traces

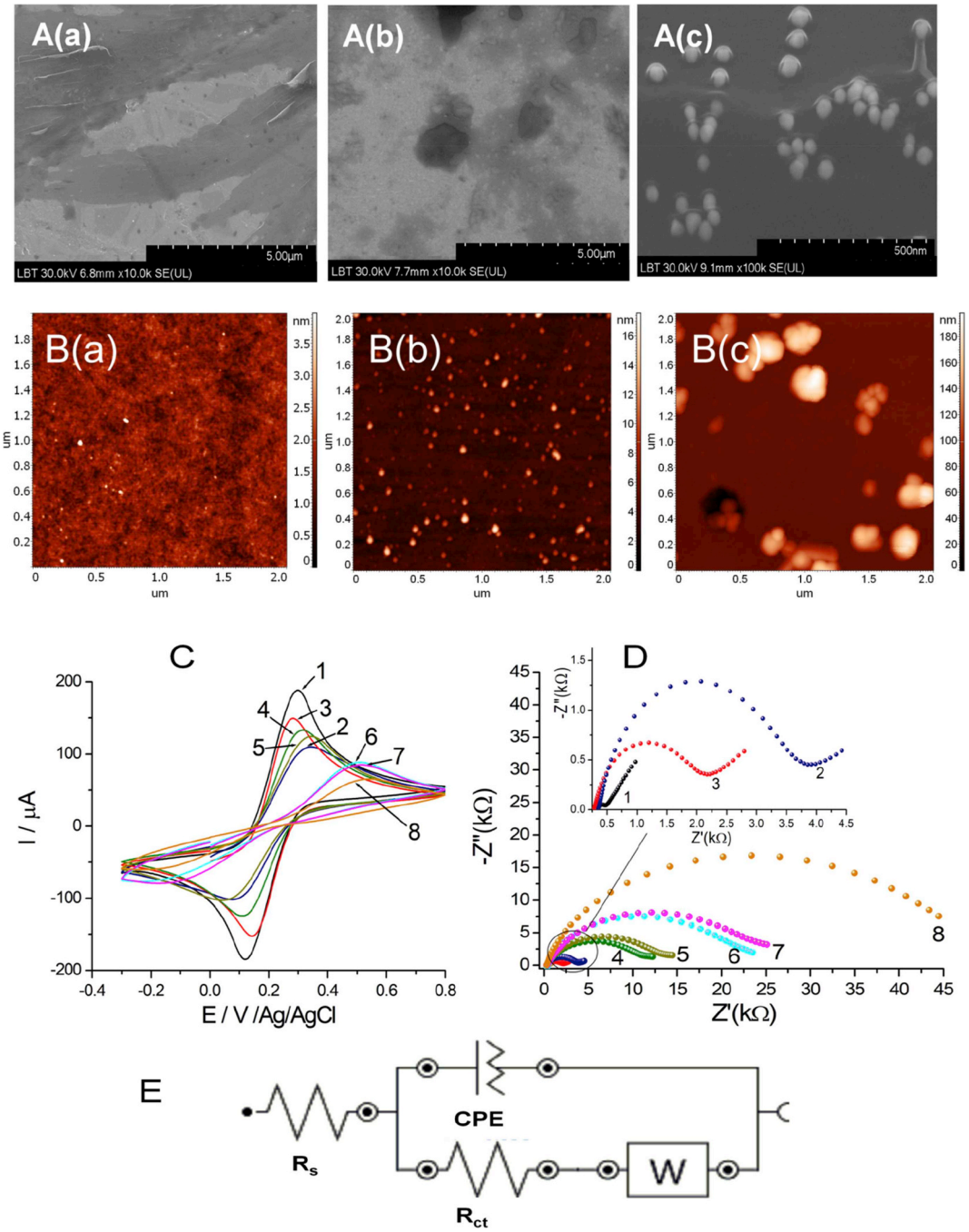

Fig. 2. A SEM images of pABA/GCE (a), pATP/pABA/GCE (b), AuNPs/pATP/pABA/GCE (c) (More details in ***Supplementary data***, Figure S2**). B.** Representative AFM topographic images of: bare GCE (a), pATP/pABA/GCE (b), AuNPs/pATP/pABA/GCE (c) (More details in ***Supplementary data***, Figure S3**). C.** CVs (10 mmol L^{-1} $[Fe(CN)_6]^{3-/4-}$ solution containing 0.1 M KCl; 50 mV s^{-1}) and **D.** EIS Nyquist graphs (5 mmol L^{-1} of $[Fe(CN)_6]^{3-/4-}$ (1:1) containing 5 mmol L^{-1} KCl; amplitude: 10 mV; frequency domain from 1 Hz to 10 kHz; OCP) for: unmodified GCE (black; 1); pABA/GCE (blue; 2); pABA/GCE after activation of –COOH groups with NHS/EDC (red; 3); pATP/pABA/GCE (green; 4); AuNPs/pATP/pABA/GCE (dark yellow; 5); Apt/AuNPs/pATP/pABA/GCE (light blue; 6); MCH/Apt/AuNPs/pATP/pABA/GCE (pink; 7) and 2 ngmL^{-1} IL-6/MCH/Apt/AuNPs/pATP/pABA/GCE (orange; 8). Inset: zoom in for high frequency domain. **E.** The equivalent electrical circuit used to fit the impedance data. (For interpretation of the references to color in this figure legend, the reader is referred to the Web version of this article.)

of thiol that were also detected. Here again the N 1*s* core-level line integral intensity is correlated with C 1*s* core-level line intensity corresponding to C–N bonding. Line positions and intensities corresponding to sample AuNPs/p-ATP/p-ABA/GCE are summarized in Table S4. Their interpretation was more difficult in this case due to the superposition of the two polymeric layers with AuNPs which causes selective attenuation of XPS lines regarding electrons extracted near the GCE surface. For instance, this process is illustrated by attenuation of C 1*s* sp^2 core-level line of this sample as compared to the other ones. Nevertheless, the data seen in Table S4 indicate that AuNPs are bound to the sulfur position of p-ATP. Thus the intensity of the gold line 4*d* 5/2 is almost the same as of the S 2*p* 3/2 line positioned at around 165 eV. This additional doublet line is attributed to the sulfur atoms bonded to the surface of the AuNPs. Additionally the S 2*p* lines corresponding to S–Au bonding have higher binding energies than thiol sulfur atoms which indicate the covalent nature of this bond.

3.3.2. Electrochemical characterization

Electrochemical behavior of the platform during the modification steps was studied by CV in a 10 mmolL^{-1} $[Fe(CN)_6]^{3-/4-}$ solution containing 0.1 mol L^{-1} KCl. Five successive cycles were performed at 50 mVs^{-1}, only the 5th for each step being presented in Fig. 2C. As can be observed, a well-defined pair of oxidation/reduction peaks is obtained for the electrochemical reversible transformation of the redox probe on GCE after cleaning (black; 1), with a peak-to-peak separation of 0.18 V and a maximum current intensity. After the immobilization of pABA a decrease in current intensity of 42% was observed, while the separation of the peaks was increased at 0.25 V (blue; 2). Peak-to-peak separation reached its minimum (0.13 V) after the activation of the carboxylic functionalities grafted at the electrode, together with an increase in the current intensity of about 36% (red; 3). Further immobilization of pATP caused a decrease in signal of about 11% and an increase in peaks separation of 0.2 V (green; 4). By contrast, the self-assembling of the AuNPs decreased the current intensity with only 5% and increased the peaks separation at 0.29 V (dark yellow; 5). The next three steps consisted in the immobilization of the Apt molecules (light blue; 6), the blocking step with MCH (pink; 7) and the immobilization of IL-6 (orange; 8) have caused a continuous drop of the current signal (with 29%, 5.8% and 23%, respectively) and an increase of the peaks separations (to 0.64 V, 0.66 V and 0.71 V, respectively). Therefore, it was obtained an increase in the coverage of the electrode surface with the biorecognition element, biocomponents and organic substances that hampered the transfer of electrons. A correlation between the recorded signal and the protein concentration used for incubation could not be performed, thus excluding the indirect voltammetric detection of IL-6.

EIS was used to evaluate the changes of the electrode surface during the modification and functionalization steps involved in aptasensor elaboration. In the Nyquist plot of EIS, the diameter of the semicircle visible at higher frequencies represents the resistance to electrons transfer, so called resistance of charge transfer (R_{ct}). Any change in the conductive properties of an electrode, regardless it is linked to its increasing or decreasing, can be observed through the variation of R_{ct}. As can be noticed in Fig. 2D and Table S5, each step of the aptasensor elaboration resulted in the increase of the R_{ct}. The impedance results were further analyzed by fitting and simulation. A Randles-type equivalent electrical circuit has been used (see the schematic representation in Fig. 2E). All the values for the kinetic parameters determined after fitting the EIS data for the applied experimental protocol are included in Table S5. The proposed circuit contains the following elements: the resistance of the solution (R_s), the resistance of charge transfer (R_{ct}), the Warburg impedance (W) which resulted from the diffusion of the negatively charged redox couple, and a constant phase element (Q = CPE). This circuit represents the equivalent model of double-layer capacitance and is usually suitable for describing the mechanism at the surface of biosensors based on composite films (Lien et al., 2010; Baraket et al., 2017).

It can be observed that after the electrochemical grafting of pABA by using the optimized CV protocol (blue; 2), the R_{ct} has registered a substantial increase from 253 Ω (in the case of bare GCE, (black; 1)) to 3787 Ω, confirming the success of the electrode grafting. The increase in the R_{ct} value may be due to the repulsion of the negatively charged $[Fe(CN)_6]^{3-/4-}$ ions by the negatively charged carboxylic groups that are obtained at the electrode surface after the electrochemical grafting of pABA, as it was observed before (Pilehvar et al., 2017; Yang et al., 2006).

The activation process of the carboxylic groups with NHS/EDC determined the decrease of R_{ct} to 1786 Ω (red; 3), probably influenced by the cancelation of the negative charge of pABA moieties after their involvement in covalent bonds with the NHS molecules in the presence of EDC. The next step of the protocol consisted in the immobilization of pATP through amidic bounds, caused the dramatic increase of R_{ct} to 10349 Ω (green; 4), and as a consequence of organic molecules self-assembling that determines the increase in the layer thickness deposited at the GCE. Further increase in R_{ct} to 13533 Ω was observed again after immobilization of AuNPs (dark yellow; 5). An almost double value for R_{ct} was registered after the immobilization of the IL-6 specific Apt (23945 Ω; (light blue; 6)), which is due to the repulsion barrier created between the negatively charged $[Fe(CN)_6]^{3-/4-}$ and the negatively charged phosphate backbones of the Apt, this phenomenon being previously observed for the same DNA oligonucleotide (Tertiş et al., 2017b). The blocking step with MCH determined an additional increase in R_{ct} to 25332 Ω (pink; 7), proving an increase in the coverage of conductive surfaces (e.g. the surface of AuNPs that was not covered with Apt units) with organic compounds. After 60 min incubation of the aptasensor with 2 ngmL^{-1} IL-6 solution, another dramatic increase in the R_{ct} was observed, this value being almost double compared with the previous step (48788 Ω (orange; 8)).

Thus, after performing CV and EIS tests it was concluded that there was a perfect correlation between the results obtained with both methods, proving the validity of the proposed strategy for the aptasensor manufacturing. Moreover, it was observed that there is a good correlation between the analyte concentration and the analytical signal, consequently, this analytical method has been successfully employed for sensor testing. All the parameters obtained after fitting the experimental data are presented in Table S5.

3.4. Analytical features of the IL-6 aptasensor

3.4.1. Linear range and limit of detection

The analytical performance of the developed aptasensor regarding the linear range and limit of detection (LOD) was evaluated by EIS. More precisely, the R_{ct} variation was determined from the Nyquist graphs after exposing the aptasensor to solutions containing different levels of IL-6. Six different concentrations of IL-6, in a wide range from 0.005 to 100 ngmL^{-1} (prepared in 0.1 mol L^{-1} PBS pH7.4), were tested and the plot of the EIS response as a function of IL-6 concentrations is revealed in Fig. 3A. It can be observed that the increase in IL-6 concentration induces an increase in EIS signal, proving the successful immobilization of the Il-6 molecules through interaction with the specific Apt. Moreover, the variation of ΔR_{ct} calculated for the increased IL-6 concentrations relatively to the R_{ct} registered in the absence of the target is characterized by a logarithmic equation (Fig. 3B). Minimum three aptasensors were elaborated and tested for each concentration considered in this study.

Different aptasensors were immersed in IL-6 solutions of different concentrations, being in contact for 60 min at 25 °C. The surface of the aptasensor was careful washed with buffer solution in order to remove the unbound protein molecules. The measurements were further performed in the presence of 5 mmolL^{-1} of $[Fe(CN)_6]^{3-/4-}$ solution prepared in 5 mmolL^{-1} KCl.

The inset of Fig. 3B presents the linear variation of the normalized ΔR_{ct} values, depending on the logarithm of the IL-6 concentration. This linear variation was valid throughout the entire range of tested concentrations, and is described by the following equation: $\Delta R_{ct}(\Omega) = 9821 \pm 78 \cdot \log([\text{IL-6}](\text{ngmL}^{-1})) + 22534 \pm 465$, with a correlation coefficient of 0.9881, demonstrating that detection errors are less than 2%. A limit of quantification (LOQ) of 5 pgmL^{-1} and a LOD of 1.6 pgmL^{-1} were estimated based on ten measurements, and three measurements, respectively, being based on the standard deviation of the blank divided by the slope of the calibration curve (Pilehvar et al., 2017; Shi et al., 2014). Considering that the cut-off levels of IL-6 in serum are in the range of 4–6 pgmL^{-1} (Yanagawa et al., 1995) for healthy individuals and are significantly increased in several pathologies, the obtained analytical parameters posse clinically significance. These results indicate that the present method can be successfully used for IL-6 detection with high sensitivity and good LOD.

The analytical parameters of the sensor were compared with other electrochemical sensors and biosensors reported in the literature. It can be observed in Table 2 that the analytical performance of the optimized

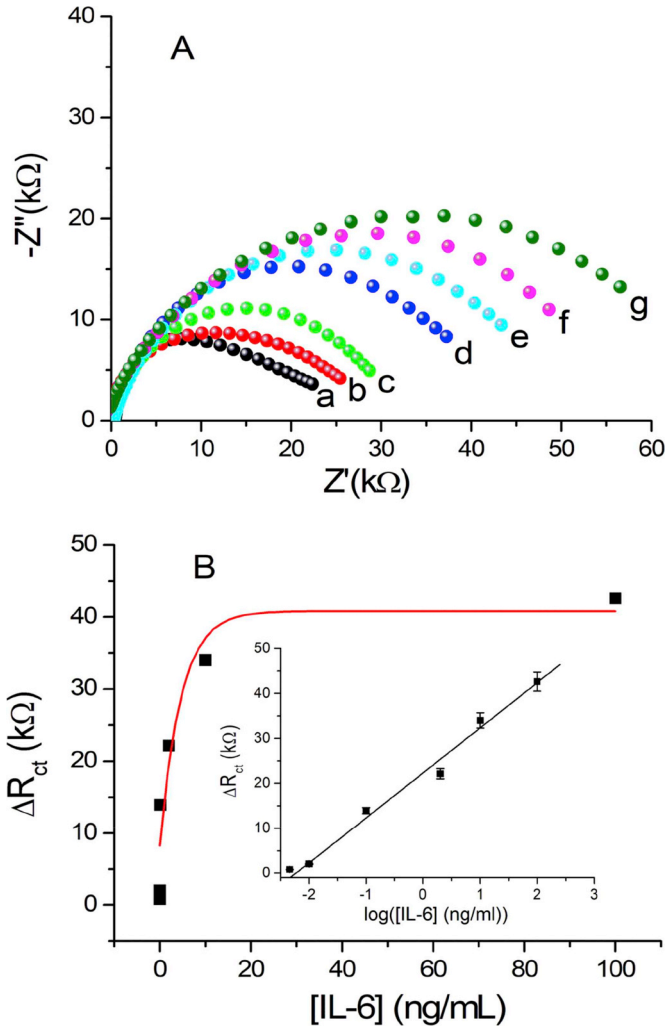

Fig. 3. (A) EIS graphs of the aptasensor corresponding to the tests obtained after 60 min incubation with different concentrations of IL-6: 0 $ngmL^{-1}$ (black; a) 5 $pgmL^{-1}$ (red; b); 10 $pgmL^{-1}$ (green; c); 0.1 $ngmL^{-1}$ (blue; d); 2 $ngmL^{-1}$ (light blue; e); 10 $ngmL^{-1}$ (pink; f); and 100 $ngmL^{-1}$ (olive; g) in 5 $mmolL^{-1}$ of $[Fe(CN)_6]^{3-/4-}$ (1:1) in 5 $mmolL^{-1}$ KCl. **(B)** Variation of the ΔR_{ct} obtained for the above mentioned IL-6 concentrations. Inset: Relative variation of ΔR_{ct} with the logarithm of IL-6 concentration (error bars were calculated as standard deviation for minimum 3 measurements on each concentration). (For interpretation of the references to color in this figure legend, the reader is referred to the Web version of this article.)

aptasensor are comparable to those reported in the literature. Moreover, the protocol used for IL-6 aptasensor elaboration is very simple and it involves low consumption of reagents, including the aptamers, taking advantage of the cumulative benefits of covalent AuNPs binding and a fast and sensitive label-free electrochemical detection strategy. These advantages along with the validation of the sensor by tests in real samples show that the proposed aptasensor can be used for the elaboration of disposable devices for clinical applications.

The high sensitivity of the designated aptasensor probably relies on the good affinity of the Apt used for this study toward IL-6 detection and the efficient protocol used for the construction of the immobilization platform.

3.4.2. Reproducibility and stability of the aptasensor

To evaluate the reproducibility of the optimized aptasensor, the inter-assay precision was investigated. For this purpose, ten different electrodes were independently modified with the same protocol and incubated with the same concentration (2 $ngmL^{-1}$) of IL-6 solution. By

Table 2
Comparison between the elaborated aptasensor and other related works on IL-6 electrochemical sensing.

Sensor configuration	Detection method	LOD (pg mL^{-1})	Dynamic range	Real samples	Ref.
Electrochemical immunosensors based on SWCNT forests and glutathione protected AuNPs	Amperometry	10	20–4000 pg mL^{-1}	serum	Munge et al. (2009)
Electrochemical immunosensor based on AuNPs-poly-dopamine and multienzyme-antibody functionalized AuNP-PDOP@CNTs	Amperometry	1	4–800 pg mL^{-1}	serum	Wang et al. (2011)
Immunosensor based on electrically heated CPE	ASV	0.033	0.1–100 pg mL^{-1}	serum	Zhang et al. (2011)
Electrochemical immunoassay based on PS@PDA-metal nanocomposites with graphene nanoribbon-modified heated carbon SPEs	SWV	0.005	0.01–0.1 pg mL^{-1}	clinical serum	Shi et al. (2014)
Electrochemical immunosensor based on ferrocene loaded porous polyelectrolyte nanoparticles with $CaCO_3$ template	SWV	1	2–20 pg mL^{-1}	serum	Li T. et al. (2011)
Electrochemical immunosensor based on AgNPs–hollow titanium phosphate sphere hybrid	DPV	0.1	0.5–10000 pg mL^{-1}	serum	Peng et al. (2011)
Photoelectrochemical immunoassay based on TiO_2/CdS/CdSe dual co-sensitized structure	PEI	0.38	1–100000 pg mL^{-1}	–	Fan et al. (2014)
Electrochemiluminescence immunosensor array featuring capture-antibody-decorated SWCNT forests	ECL	0.25	0.1–1000 pg mL^{-1}	serum	Sardesi et al. (2011)
Electrochemical immunosensor based on electrochemically deposited AuNPs a SiO_2/Si substrate	EIS	0.00001	0.01–100 fg mL^{-1}	serum	Yang et al. (2013)
Electrochemical aptasensor based on gold electrode modified with AuNPs	EIS	0.02	0.02–20 pg mL^{-1}	sweat	Selva Kumar et al. (2016)
Electrochemical aptasensor, based on a carbon SPEs modified with Ppy and AuNPs	EIS	0.33	1-15000000 $pgmL^{-1}$	serum	Tertiş et al. (2017b)
Electrochemical magnetoimmunosensor based on protein G modified magnetic nanoparticles	EIS	0.33	1–100000 pg mL^{-1}	serum	Tertis et al. (2019)
Electrochemical aptasensor based on GCE modified with *p*-ABA, *p*-ATP and AuNPs	EIS	1.66	5–100000 pg mL^{-1}	clinical serum	This study

ASV = Anodic stripping voltammetry; SWV = Square wave voltammetry; DPV = differential pulse voltammetry; PEI = Photo electrochemical immunoassay; ECL = Electrochemiluminescence; EIS = Electrochemical impedance spectroscopy; AuNPs = gold nanoparticles; AgNPs = silver nanoparticles;.

using the EIS data obtained after testing these aptasensors, an RSD of 5.1% was calculated, suggesting acceptable reproducibility and indicating that the variation of the results obtained with different aptasensors can be considered negligible. The long term storage stability of the aptasensor is very important feature for the envisaged practical applications. This feature was studied for one month, testing minimum three aptasensors for each situation considered for this study. In detail, different aptasensors were prepared in the same day, after 7, 14 and 28 days, after 60 min incubation with the same concentration (2 ngmL^{-1}) of IL-6 solution. It was observed that 93% of the initial signal was retained after 7 days, 89% after 14 days, and 81% after 28 days, proving good storage capability for the aptasensing platform, and the stability of the Apt configuration suitable for the affinity reaction with the target protein. This may be due to the presence of AuNPs on the electrode that allows the covalent immobilization and stabilization of the Apt while maintaining their activity.

3.4.3. Selectivity of the aptasensor for IL-6 detection

An electrochemical aptasensor designed for practical applicability has to prove acceptable selectivity. The selectivity of the proposed aptasensor toward IL-6 was evaluated in the presence of four proteins, namely: carcinoembryonic antigen (CEA), Mucin 1 (MUC1), Mucin 4 (MUC4) and Mucin 16 (Muc16). The ability of this Apt to selectively capture and bind the target was previously studied and confirmed (Tertiş et al., 2017b). Different aptasensors (minimum three aptasensors for each situation considered for this study) have been incubated with the mentioned proteins using 100-fold more concentrated solutions, compared with concentration used for IL-6 (2 ngmL^{-1}). As presented in Fig. 4A (red; 2), a significant increase in the EIS signal was observed as a consequence of the specific interaction between IL-6 and its Apt, compared to the signal obtained in the absence of the protein (black; 1). On the contrary, when the interfering species were tested, the variation of the R_{ct} was not so significant (see the caption of Fig. 4 for assigning the EIS curves corresponding to each protein used in this study).

Thus, the percentage influence on the analytical signal obtained with the developed sensor can be seen in Fig. 4B: 8.5% (RSD = 4.3) for CEA (green), +11.4% (RSD = 4.8%) for MUC1 (blue); 23.3% (RSD = 3.7%) for MUC4 (light blue) and 3.5% (RSD = 2.6%) for MUC16 (pink), respectively.

In addition to this, another control experiment was carried out emphasizing and confirming the selectivity of the Apt in the presence of IL-6. In this case, the sensor was tested, verifying the EIS signals obtained after using a randomly chosen DNA oligonucleotide (see details about this DNA in *Supplementary data*). The obtained results showed that only a smaller change in R_{ct} was registered when the random DNA oligonucleotide was immobilized on the modified electrode Fig. 4A (dark yellow, 7). Therefore, based on these observations, it can be assumed that almost no interaction can be noticed between the control DNA and the target, confirming that the proposed strategy enables the selective detection of IL-6.

3.4.4. Application in analysis of real samples

The assessment of the aptasensor capabilities with real samples (such as blood) has to be demonstrated in order to prove their practical applicability, giving further possibility in miniaturization, multiplexing, design and fabrication of point-of-care devices.

The blood samples were collected from three patients suffering from colorectal cancer. The supernatant obtained after centrifugation (serum) was collected and placed in sterilized plastic containers for further electrochemical investigations. Initial tests were carried out on undiluted serum, but the recovery levels were low. Thus, prior to testing, serum samples were 1:1 diluted with 0.1 mol L^{-1} PBS pH7.4. Subsequently, 15 µL of diluted solutions were deposited on the surface of the sensor and incubated for 60 min at 25 °C in humid environment to avoid solvent evaporation. In the next step, the sensors were rinsed

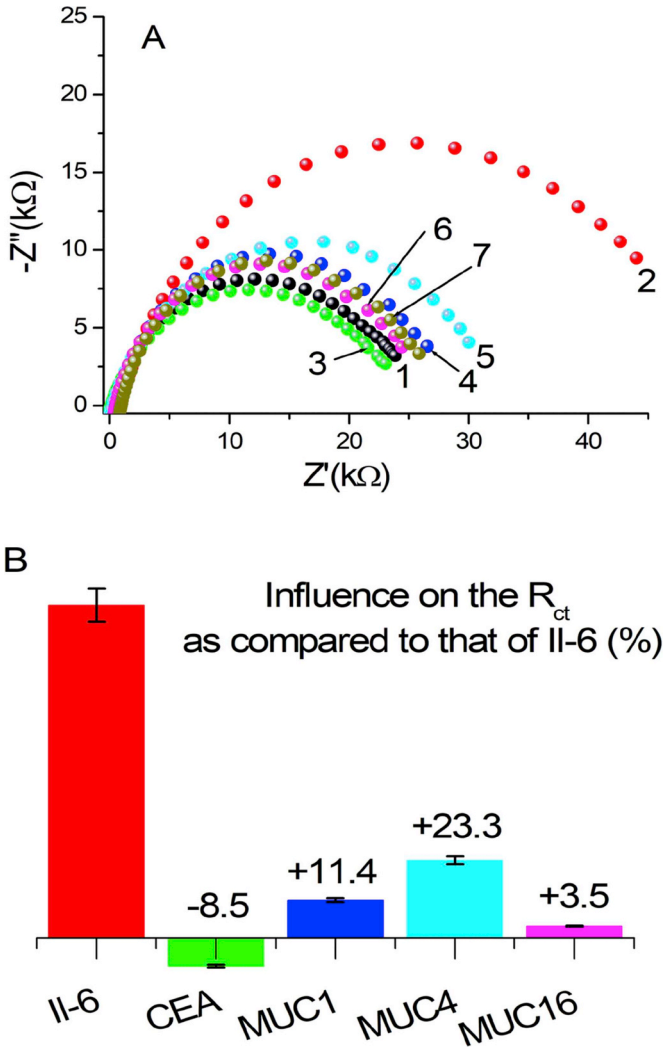

Fig. 4. (A) EIS responses and **(B)** the influence on the R_{ct} of the optimized aptasensor in the presence of 2 ngmL^{-1} IL-6 (red; 2); and 200 ngmL^{-1} of CEA (green; 3); MUC1 (blue; 4); MUC4 (light blue; 5); and MUC 16 (pink; 6) compared with the EIS signal obtained on the aptasensor in the absence of any protein (black; 1) ((60 min incubation with serum and Il-6 spiked serum at 25 °C; tests performed in 5 mmolL^{-1} of $[Fe(CN)_6]^{3-/4-}$ (1:1) in 5 mmolL^{-1} KCl. EIS signal obtained on the optimized platform modified with a random chosen Apt after incubation with 2 ngmL^{-1} IL-6 is also presented in **Figure (A)** (dark yellow; 7). (For interpretation of the references to color in this figure legend, the reader is referred to the Web version of this article.)

with buffer and tested by EIS in 5 mmolL^{-1} $[Fe(CN)_6]^{3-/4-}$ solution prepared in 5 mmolL^{-1} KCl, according to the optimized protocol. Recovery tests were also carried out using standard addition method in 1:1 diluted sample of serum, after addition of the precise volume from a 1 mgmL^{-1} IL-6 stock solution (the final protein concentration was 2 ngmL^{-1}). EIS tests of the aptasensor were performed after incubation with 15 µL of the spiked serum sample. The results obtained are shown in Table 3.

Based on the dilution performed, the initial IL-6 concentration found using the optimized aptasensing platform was in the range 4.2–9.6 pgmL^{-1} in the considered serum samples (Table 3). Several studies have been performed for investigation of the IL-6 levels and the effects on the prognosis, stage, cancer treatment outcome and relapse (Chang et al., 2013). In the case of patients suffering of lung cancer, an average value of 36.54 pgmL^{-1} was estimated for IL-6 *versus* 4 pgmL^{-1} for controls. In comparison, for the patients suffering of colorectal cancer, the cut-off level of IL-6 was found to be increased during the

Table 3
The levels of IL-6 found in serum collected from patients with colorectal cancer and recoveries obtained from EIS data recorded with the developed aptasensor, compared with those obtained with CLIA.

Serum sample	IL-6 concentration (pg mL^{-1})		
	Aptasensor (EIS)[a]	RSD (%)	CLIA[b]
Patient 1	4.2	4.1	4.6
Patient 2	6.8	3.8	6.0
Patient 3	9.6	2.7	8.8

Serum sample	Added IL-6 (pg mL-1)	Found IL-6 (pg mL-1)	Recovery (%)	RSD (%)
Patient 1	2000	2156 ± 56	107.5	2.6
Patient 2	2000	2086 ± 64	103.9	3.1
Patient 3	2000	2204 ± 33	109.6	1.5

[a] EIS: electrochemical impedance spectroscopy. [b] CLIA – chemiluminescence immunoassay.

treatment at 4.2 $pgmL^{-1}$ (average IL-6 level of 13.2 $pgmL^{-1}$) *versus* 2.1 $pgmL^{-1}$ for controls (Xu et al., 2016). Mean IL-6 serum level of patients with head and neck squamous cell carcinoma is around 20 $pgmL^{-1}$ or greater, compared to a maximum level 6 $pgmL^{-1}$ or less in healthy individuals (Tertiş et al., 2017b).

An additional method, namely chemiluminescence immunoassay (CLIA) was used for this study for testifying the validation of the proposed aptasensor. The CLIA tests were performed in a laboratory accredited for clinical trials on serum samples collected from the same three patients, at the same time as those used for the practical validation of the aptasensor. The results received from this laboratory are presented as well in Table 3. The standard addition method was also applied in this scenario, and as it can be observed in Table 3, after the addition of standard IL-6 solution, the data obtained for serum are in good agreement with the given concentration, the average recoveries being of 107% (n = 3), whereas the RSD value was below 2.4%. Thus, it can be confirmed that the interferences present in the serum have negligible effect upon the detection of IL-6. Taking into account these promising experimental results and the information previously presented from the literature, it can be stated that the developed electrochemical aptasensor has promising features for the practical use and can be applied for IL-6 detection in real samples from colorectal cancer patients. However, the results presented here refer to a very small group of subjects, and cannot be extrapolated for the general population. Further studies with larger number of cohorts involved should be followed to obtain statistically relevant results.

4. Conclusions

A novel sensitive and highly selective sandwich-type electrochemical aptasensors for interleukin-6 protein has been successfully elaborated in this study. The sensor has been built step by step, resulting in a composite platform based on glassy carbon electrode modified with *p*-aminobenzoic acid, *p*-aminothiophenol and gold nanoparticles. The strategy used for electrode functionalization assured the stable and reproducible immobilization of the AuNPs which had the role in the amplification of the analytical signal. Moreover, this strategy helped in expanding the electrochemically active area and the number of the active sites available for the immobilization of the aptamer, specific for the target protein. The analytical figures of merit of this aptasensor were compared with other biosensors previously reported for the detection of human interleukin-6 cancer biomarker. The AuNPs/pATP/pABA/GCE based aptasensor offered a detection limit of 1.66 pg mL^{-1} (about 83 amol mL^{-1}) which is sufficient enough for tests real samples, taking into account that the cut-off levels of IL-6 in serum are in the range of 4–6 $pgmL^{-1}$ (Yanagawa et al., 1995) for healthy subjects and there are significant increases in disease conditions. Thus, the elaborated aptasensor possess clinically significance and was successfully applied for the detection and quantification of IL-6 in serum collected from colorectal cancer patients, the results obtained being validated by CLIA tests carried out in an accredited laboratory.

Compared to the results reported previously for IL-6 electrochemical detection, the proposed aptasensor exhibited comparable and lower detection limit. There are previous examples of sensors with a lower detection limit, but in these situations no tests have been performed on clinical samples, as in our study (see Table 2).

The strengths of the proposed sensing device are multiple, such as label-free detection, simple experimental protocol, high selectivity and low limit of detection. The optimized aptasensor proved to be a sensitive and reproducible platform with a stable and robust structure suitable for the envisaged purpose. Due to easy preparation and significant signal amplification, this elaboration strategy can be applied also for detecting other biomarkers with clinical relevance, and has the potential for reliable prediction of cancer and other diseases. This versatile platform can be considered a starting point in developing miniaturized sensors and point-of-care devices.

CRediT authorship contribution statement

Mihaela Tertis: Conceptualization, Investigation, Writing - original draft. **Petrica Ionut Leva:** Investigation, Validation. **Diana Bogdan:** Methodology, Formal analysis. **Maria Suciu:** Methodology, Formal analysis. **Florin Graur:** Investigation, Data curation, Resources, Writing - review & editing, Funding acquisition. **Cecilia Cristea:** Conceptualization, Resources, Writing - review & editing, Visualization, Supervision, Funding acquisition, Project administration.

Acknowledgements

The authors are grateful for the financial support from the Romanian National Authority for Scientific Research and Innovation, CNCS/CCCDI-UEFISCDI; project number PN-III-P1-1.2-PCCDI2017-0221, within PNCDI III. D. Bogdan acknowledges financial support from the Romanian National Authority for Scientific Research and Innovation (ANCSI) through the Core Program, Project PN18-03 02 01. The authors acknowledge Dr. Ovidiu Pană (National Institute for Research and Development of Isotopic and Molecular Technologies, Cluj-Napoca, Romania) for XPS experiments and their interpretation.

Appendix A. Supplementary data

Supplementary data to this article can be found online at https://doi.org/10.1016/j.bios.2019.05.012.

Declaration of interests

The authors declare that they have no known competing financial interests or personal relationships that could have appeared to influence the work reported in this paper.

References

Amiri, M., Akbari, A., Ahmadi, M., Pardakhti, A., Salavati-Niasari, M., 2018a. J. Mol. Liq. 249, 1151–1160.
Amiri, M., Pardakhti, A., Ahmadi-Zeidabadi, M., Akbari, A., Salavati-Niasari, A., 2018b. Colloids Surf., B 172, 244–253.
Baraket, A., Lee, M., Zine, N., Sigaud, M., Bausells, J., Errachid, A., 2017. Biosens. Bioelectron. 93, 170–175.
Cernat, A., Tertiş, M., Săndulescu, R., Bedioui, F., Cristea, A., Cristea, C., 2015. Anal. Chim. Acta 886, 16–28.
Cernat, A., Tertis, M., Gandouzi, I., Bakhrouf, A., Suciu, M., Cristea, C., 2018. Electrochem. Commun. 88, 5–9.
Chang, C.H., Hsiao, C.F., Yeh, Y.M., Chang, G.C., Tsai, Y.H., Chen, Y.M., et al., 2013. Int. J. Cancer 132, 1977–1985.
Chen, P., Chung, M.T., McHugh, W., Nidetz, R., Li, Y., Fu, J., Cornell, T.T., Shanley, T.P., Kurabayashi, K., 2015. ACS Nano 9, 4173–4181.
Chen, H.-J., Chen, R.L.C., Hsieh, B.-C., Hsiao, Hsien-Yi, Kung, Y., Hou, Y.-T., et al., 2019. Biosens. Bioelectron. 131, 53–59.
Erdem, A., 2007. Talanta 74, 318–325.
Fan, G.C., Ren, X.L., Zhu, C., Zhang, J.R., Zhu, J.J., 2014. Biosens. Bioelectron. 59, 45–53.
Fayad, L., Keating, M.J., Reuben, J.M., O'Brian, S., Lee, B.-N., Lerner, S., et al., 2001. Blood 97 (1), 256–263.
Fritea, L., Le Goff, A., Putaux, J.-L., Tertis, M., Cristea, C., Săndulescu, R., Cosnier, S., 2015a. Electrochim. Acta 178, 108–112.
Fritea, L., Tertiş, M., Cosnier, S., Cristea, C., Săndulescu, R., 2015b. Int. J. Electrochem. Sci. 10, 7292–7302.
Gobbo, P., Ghiassian, S., Hesari, M., Stamplecoskie, K.G., Kazemi-Zanjani, N., Lagugne-Labarthet, F., Workintin, M.S., 2012. J. Mater. Chem. 22, 23971–23980.
Gold, L., Ayers, D., Bertino, J., Bock, C., Bock, A., Brody, E.N., et al., 2010. PLoS One 5, e15004.
Gupta, S., Thirstrup, D., Jarvis, T.C., Schneider, D.J., Wilcox, S.K., Carter, J., et al., 2011. Med. Mol. Morphol. 19, 273–278.
Gupta, S., Hirota, M., Waugh, S.M., Murakami, I., Suzuki, T., Muraguchi, M., et al., 2014. J. Biol. Chem. 289 (12), 8706–8719.
Hanash, S.M., Pitteri, S.J., Faca, V.M., 2008. Nature 452, 571–579.
Hendricks, H.A., Kortlandt, W., Verweij, W.M., 2000. Clin. Chem. 46, 105–111.
Huang, Q., Liu, M., Chen, J., Wan, Q., Tian, J., Huang, L., et al., 2017. Appl. Surf. Sci. 419, 35–44.
Kumari, N., Dwarakanath, B.S., Das, A., Bhatt, A.N., 2016. Tumor Biol. 37 (9), 11553–11572.
Lagiou, P., Trichopoulos, D., 2011. JNCI. J. Natl. Cancer Inst. 103, 1073–1075.
Le Saout, C., Lane, H.C., Catalfamo, M., 2012. Cytokine Growth Factor Rev. 23, 207–214.
Li, T., Yang, M.H., 2011. Sensor. Actuator. B Chem. 158, 361–365.
Lien, T.T.N., Lam, T.D., An, V.T.H., Hoang, T.V., Quang, D.T., Khieu, D.Q., et al., 2010. Talanta 80, 1164–1169.
Liu, G., Qi, M., Hutchinson, M.R., Yang, G., Goldys, E.M., 2016. Biosens. Bioelectron. 79, 810–821.
Amiri, M., Salavati-Niasari, M., Akbari, A., 2017. Microchim. Acta 184, 825–833.
Malhotra, R., Patel, V., Vaque, J.P., Gutkind, J.S., Rusling, J.F., 2010. Anal. Chem. 82 (8), 3118–3123.
Mazerie, I., Didier, P., Razan, F., Hapiot, P., Coulon, N., Girard, A., et al., 2018. ChemElectroChem 5, 144–152.
Mazloum-Ardakani, M., Tavakolian- Ardakani, Z., Sahraei, N., Moshtaghioun, S.M., 2019. Biosens. Bioelectron. 129, 1–6.
Mohandes, F., Salavati-Niasari, M., 2014. Mater. Sci. Eng. C 40, 288–298.
Munge, B.S., Krause, C.E., Malhotra, R., Patel, V., Gutkind, J.S., Rusling, J.F., 2009. Electrochem. Commun. 11, 1009–1012.
Peng, J., Feng, L.N., Ren, Z.J., Jiang, L.P., Zhu, J.J., 2011. Small 20, 2921–2928.
Pilehvar, S., Reinemann, C., Bottari, F., Vanderleyden, E., Van Vlierberghe, S., Blust, R., et al., 2017. Sensor. Actuator. B Chem. 240, 1024–1035.
Pine, S.R., Mechanic, L.E., Enewold, L., Chaturvedi, A.K., Katki, H.A., Zheng, Y.L., et al., 2011. JNCI. J. Natl. Cancer Inst. 103, 1112–1122.
Qazi, U.Y., Javaid, R., 2016. Adv. Nanoparticles 5, 27–43.
Roushani, M., Shahdost-fard, F., 2015. Talanta 144, 510–516.
Sardesai, N.P., Barron, J.C., Rusling, J.F., 2011. Anal. Chem. 83, 6698–6703.
Selva Kumar, L.S., Wang, X., Hagen, J., Naik, R., Papautsky, I., Heikenfeld, J., 2016. Anal. Methods 8, 3440–3444.
Shi, J.J., Ting, T., Jiang, F., Abdel-Halim, E.S., Zhu, J.J., 2014. Biosens. Bioelectron. 55, 51–56.
Shin, H., Kang, C., 2003. Anal. Sci. 19, 1667–1670.
Tertiş, M., Florea, A., Săndulescu, R., Cristea, C., 2013. Sensors 13 (4), 4841–4854.
Tertis, M., Cernat, A., Lacatis, D., Florea, A., Bogdan, D., Suciu, M., et al., 2017a. Electrochem. Commun. 75, 43–47.
Tertiş, M., Ciui, B., Suciu, M., Săndulescu, R., Cristea, C., 2017b. Electrochim. Acta 258, 1208–1218.
Tertis, M., Florea, A., Adumitrachioaie, A., Cernat, A., Bogdan, D., Barbu-Tudoran, L., et al., 2017c. ChemPlusChem 82, 561–569.
Tertis, M., Melinte, G., Ciui, B., Simon, I., Stiufiuc, R., Sandulescu, R., Cristea, C., 2019. Electroanalysis 31, 282–292.
Wang, G., Huang, H., Zhang, G., Zhang, X., Fang, B., Wang, L., 2011. Langmuir 27, 1224–1231.
Xu, J., Ye, Y., Zhang, H., Szmitkowski, M., Makinen, M.J., Li, P., et al., 2016. Medicine 95 (2). https://doi.org/10.1097/MD.0000000000002502.
Xue, Q., Lu, Y., Eisele, M.R., Sulistijo, E., Fan, R., Miller-Jensen, K., 2015. Sci. Signal. 8 (381), ra59.
Yanagawa, H., Sone, S., Takahashi, Y., Haku, T., Yano, S., Shinohara, T., Ogura, T., 1995. Br. J. Canc. 71 (5), 1095–1098.
Yang, G., Shen, Y., Wang, M., Chen, H., Liu, B., Dong, S., 2006. Talanta 68, 741–747.
Yang, T., Wang, S., Jin, H., Bao, W., Huang, S., Wang, J., 2013. Sensor. Actuator. B Chem. 178, 310–315.
Yang, S., Zhang, F., Liang, Q., Wang, Z., 2018. Biosens. Bioelectron. 120, 85–92.
Zarogoulidis, P., Yarmus, L., Darwiche, K., Walter, R., Huang, H., Li, Z., et al., 2013. Immunome Res. 9 (62), 16535.
Zhang, L., Jiang, X., Wang, E., Dong, S., 2005. Biosens. Bioelectron. 21, 337–345.
Zhang, J.J., Liu, Y., Hu, L.H., Jiang, L.P., Zhu, J.J., 2011. Chem. Commun. 47, 6551–6553.
Zhang, X., Servos, M.R., Liu, J., 2012. J. Am. Chem. Soc. 134 (17), 7266–7269.
Zhang, X., Huang, Q., Deng, F., Huang, H., Wan, Q., Liu, M., et al., 2017. Appl. Mater. Today. 7, 222–238.
Zinatloo-Ajabshir, S., Salavati-Niasari, M., Sobhani, A., Zinatloo-Ajabshir, Z., 2018. J. Alloy. Comp. 767, 1164–1185.